Modeling and measurement of tissue elastic moduli using Optical Coherence Elastography

Xing Liang[1], Amy L. Oldenburg[1], Vasilica Crecea[2], Sureshkumar Kalyanam[3], Michael F. Insana[3], Stephen A. Boppart[1]

[1]Department of Electrical and Computer Engineering, [2]Department of Physics, [3]Department of Bioengineering, Beckman Institute for Advanced Science and Technology, University of Illinois at Urbana–Champaign, Urbana, IL

ABSTRACT

Mechanical forces play crucial roles in tissue growth, patterning and development. To understand the role of mechanical stimuli, biomechanical properties are of great importance, as well as our ability to measure biomechanical properties of developing and engineered tissues. To enable these measurements, a novel non-invasive, micron-scale and high-speed Optical Coherence Elastography (OCE) system has been developed utilizing a titanium:sapphire based spectral-domain Optical Coherence Tomography (OCT) system and a mechanical wave driver. This system provides axial resolution of 3 microns, transverse resolution of 13 microns, and an acquisition rate as high as 25,000 lines per second. External low-frequency vibrations are applied to the samples in the system. Step and sinusoidal steady-state responses are obtained to first characterize the OCE system and then characterize samples. Experimental results of M-mode OCE on silicone phantoms and human breast tissues are obtained, which correspond to biomechanical models developed for this analysis. Quantified results from the OCE system correspond directly with results from an indentation method from a commercial. With micron-scale resolution and a high-speed acquisition rate, our OCE system also has the potential to rapidly measure dynamic 3-D tissue biomechanical properties.

KEYWORDS: Optical coherence elastography, tissue phantom, silicone, Young's modulus

1. INTRODUCTION

Mechanical forces and biomechanical properties play a significant role in biological tissue development, organization, and response to stimuli. For living tissues, biomechanical properties depend on their molecular building blocks and can shape and modify the cellular and extracellular structures under stress[1]. Mechanical changes can influence tissue cell migration and tissue pattern[2]. It has also been known that forces of adhesion between particular layers of cells may regulate the growth of tissues[3]. Therefore, to understand and measure tissues biomechanical properties under mechanical stimuli is of great importance.

Atomic force microscope can be used to determine the biomechanical properties of soft tissues[4]. However, according to the tissue models, strict boundary conditions should be considered in the measurement. And also, the error estimated in this method was rather high. Diffusing wave spectroscopy is another way to determine tissue biomechanical properties[5]. But experiments done on real tissue *in vivo* have not been shown in this method.

Ultrasound elastography was the first imaging technology to perform elastography and is widely used in medical diagnostic applications to image the biomechanical properties of soft tissues[6]. However, in ultrasound, the typical imaging resolution is between 125 and 200 μm[7]. Optical coherence elastography (OCE) is a novel technology determining tissue biomechanical properties utilizing Optical Coherence Tomography (OCT). The idea of OCE is similar to ultrasound elastography except that it is hard to mechanically stimulate soft tissues by optical beams. Thus, the stimuli to the tissues are usually run by mechanical devices. Also, cross-correlation algorithms are needed to quantify the

Optics in Tissue Engineering and Regenerative Medicine II, edited by Sean J. Kirkpatrick, Ruikang K. Wang, Proc. of SPIE Vol. 6858, 685803, (2008) · 1605-7422/08/$18 · doi: 10.1117/12.760779

displacements[8-11]. Compared with ultrasound elastography, OCE can perform higher resolution, which can be as high as several microns in axial direction and the acquisition rate can be as high as 370k lines/s[12]. In this paper, we propose a novel OCE system to measure elastic moduli of tissues phantoms using low-frequency vibration method without cross-correlation algorithm.

2. MATERIALS AND METHODS

Tissue Phantom Preparation

Tissue phantoms were used to calibrate the elastic moduli measurements by OCE system because of their similar optical scattering and biomechanical properties to real tissues. Silicone-based phantoms were chosen due to the ability to vary the elastic moduli and remain stable under room temperature[13]. The phantoms were fabricated by using pure polydimethylsiloxane (PDMS) fluid (50 cSt viscosity, ClearCo, Inc.), a room-temperature vulcanizing silicone and its associated curing agent (General Electric RTV-615 A and B, respectively, Circuit Specialists, Inc.). To obtain different elastic moduli, a series of phantoms were fabricated with different concentration ratios of these three ingredients, which are listed in Table 1. TiO_2 microparticles (Sigma-Aldrich, #224227) were embedded in the phantoms as scatterers for OCT imaging at a concentration of 1 mg/g, which is proper for tracking the particles by OCT. The phantom solutions were mixed thoroughly in sonicator for 30 minutes under room temperature and then fully poured into 35 mm plastic petri dishes. All the phantoms were cured under 80°C for 8 hours and then under room temperature for 24 hours. Two groups of phantoms were fabricated identically for different measurements.

Young's Moduli Measurement by Indentation Method

Bounded indentation experiments were used to determine Young's moduli of the phantoms. A steel sphere with radius of 6.35 mm and a TA.XT Plus Texture Analyzer (Texture Technologies Corp., Algonquin, IL) were used to perform the measurements. With indenter velocity of 0.01 mm/s and displacement of 2mm, the measurements were performed for two cycles for each phantom under room temperature. A corrected Hertz contact mechanics model was used to calculate Young's Moduli of the group of phantoms (4).

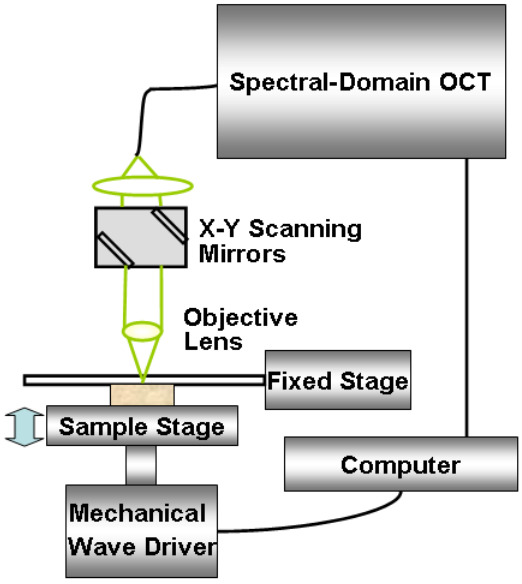

Figure 1. Schematic diagram of the OCE system. The sample stage is driven upward against a fixed optically-clear stage by the mechanical wave driver. Step or sinusoidal mechanical displacements are synchronized with the OCE acquisition system.

OCE Setup

Our OCE system has been developed based on a spectral-domain OCT. In this OCT system, the low-coherence light source consists of a Nd:YVO_4-pumped titanium:sapphire laser, which has a center wavelength of 800 nm and a bandwidth of 100 nm. A 12.5 mm diameter 40 mm focal length lens was used in the sample arm to provide an axial resolution of 3 μm and transverse resolution of 13 μm. The average power on the samples was 10 mW. A line camera was used to detect the signal with an acquisition rate of 25 kHz. As shown in Figure 1, a glass stage was fixed under the sample arm of the OCE system to present the upper boundary of samples. The sample stage was mounted on a mechanical wave driver (SF-9324, PASCO scientific, Roseville, CA), which provided a frequency range of 0.1 Hz to 5 kHz and a maximum amplitude of 7 mm at 1 Hz, decreasing with increasing frequency. The driving waveform was programmed and synchronized with the acquisition software. Samples were mounted between the upper glass window and the sample stage, with only minimal contact and force prior to data acquisition. To perform M(motion)-mode OCE, optical backscattering signals were acquired through the upper glass window (Figures 2A, B and C) while the driving mechanical perturbations were exerted simultaneously through the sample stage, compressing the sample vertically. Step and sinusoidal wave forms were used in the OCE experiments.

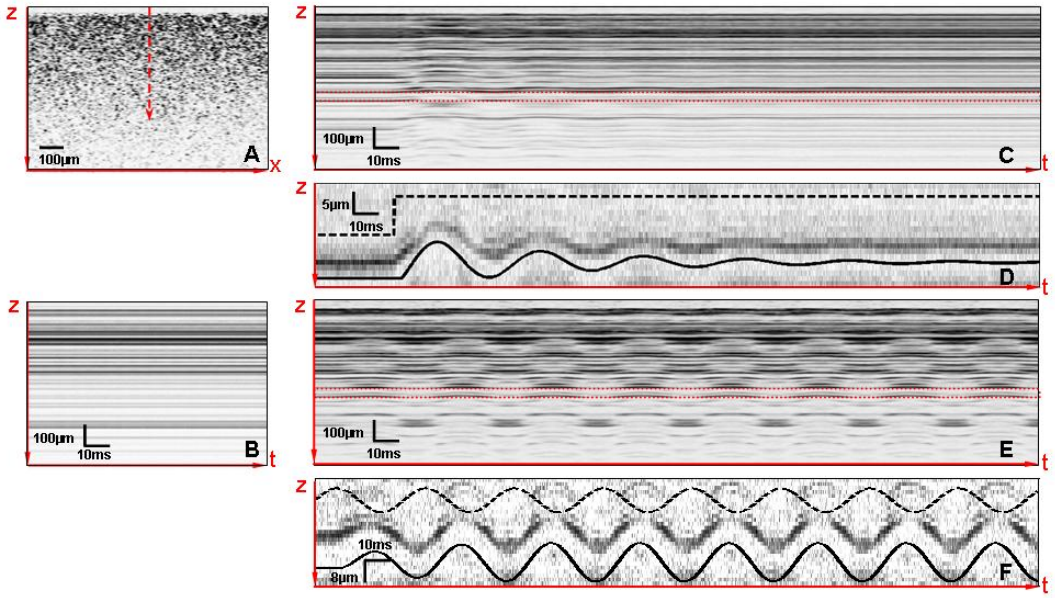

Figure 2. OCE images on silicone phantoms. (A) B-mode OCT image of one silicone phantom. Dashed arrow denotes the position of the laser beam for M-mode OCT imaging. (B) M-mode OCT image of the silicone phantom at the laser beam position in (A). (C) M-mode OCE image with a step driving waveform. (D) Zoomed-in image of the dotted range in (C). The dotted line represents the driving waveform and the solid line represents the fitted curve, while image data between the curves is due to the scattering particle movement. (E) M-mode OCE image with a sinusoidal driving waveform. (F) Zoomed-in image of the dotted range in (E).

Modeling and Young's Moduli Measurements by OCE

To describe the characteristics of both the OCE system and the samples, mechanical modeling methods were developed. First, a Voigt body was used to model the mechanical wave driver with a spring constant k_0 and a coefficient of viscosity γ_0 (Figure 3A), representing the components of the coil speaker. To quantify k_0 and γ_0, we performed M-mode OCE directly on the sample stage without any sample. This process can be described by

$$m\ddot{x} + \gamma_0\dot{x} + k_0 x = F - mg\,, \qquad [1]$$

in which m is the mass of sample stage and F is the driving step or sinusoidal force. With the OCE image, we plotted the vibration curve of the sample stage using a spline algorithm and fit the curve using the solution to Eq.1. When F is a constant or the driving force is a step wave, the solution to Eq.1 is

$$x(t) = Re^{\lambda t}\cos(\mu t - \delta), \quad [2]$$

in which R is the amplitude of the vibration, $\lambda = -\gamma_0 / 2m$ is the damping coefficient and $\mu = \sqrt{4mk_0 - \gamma_0^2}\,/\,2m$ is the natural frequency of the mechanical wave driver. Then with fitting parameters μ and λ, we can determine the spring constant $k_0 = (\mu^2 + \lambda^2)m$ and the coefficient of viscosity $\gamma_0 = -2m\lambda$. When F is a sinusoidal driving force, the solution of Eq.1 is

$$x(t) = Re^{\lambda t}\cos(\mu t - \delta) + D\sin(\omega t - \alpha), \quad [3]$$

where D and ω are the amplitude and frequency of the driving force, respectively and α is the phase shift of the vibration. With these fitting parameters, we can determine the spring constant $k_0 = (\omega^2 - \frac{2\omega\lambda}{\tan\alpha})m$ and coefficient of viscosity $\gamma_0 = -2m\lambda$.

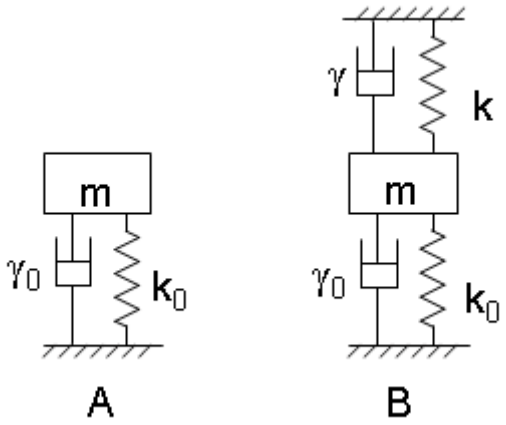

Figure 3. Mechanical models. (A) Voigt body model for the mechanical wave driver. (B) Voigt body models for mechanical wave driver and tissue or silicone phantom.

Second, the silicone phantoms were also modeled as Voigt body and incorporated into the model (Figure 3B). We sectioned the silicone phantoms into cubes of dimension approximately 10 mm × 10 mm × 16 mm to perform M-mode OCE on these discrete samples. Figure 2C is a representative of M-mode OCE image of a silicone phantom with a step driving force. From the acquired backscattered data, the dynamic motion of a single scattering particle was selected and displayed in the zoomed-in image in Figure 2D. In this figure the dashed line denotes the driving wave form and the solid line denotes the fitted curve based on the displacement and track of the real particle motion, which is shown between the dashed and solid curves. The model therefore can be described by

$$m\ddot{x} + (\gamma_0 + \gamma)\dot{x} + (k_0 + k)x = F - mg, \quad [4]$$

where k is the spring constant of the samples, γ is the coefficient of viscosity of the samples and m denotes the mass of sample stage and samples. In the same way, we can calculate the parameter k_0+k and finally solve the Young's moduli of the phantoms by

$$E_m = kL / S = [(\mu^2 + \lambda^2)m - k_0]L / S, \quad [5]$$

where L and S are thickness and contact area of the samples, respectively. This is the Young's modulus measured by the step response in OCE. Figure 2E is an OCE image of the silicone phantom with a sinusoidal driving force. Before acquiring the OCE image, we applied the sinusoidal force on the samples for 2 minutes, which enabled the sample to reach a more stable dynamic response. In Figure 2F, a zoomed in region of on particle motion is shown, along with a plot of the driving wave form and fitted curve. Then, using the similar method, Young's modulus

$$E_s = kL / S = [(\omega^2 - \frac{2\omega\lambda}{\tan\alpha})m - k_0]L / S \quad [6]$$

can be measured by sinusoidal response OCE.

Third, real tissues were modeled using the same process as for the silicone phantoms and the calculations of Young's moduli were determined in the same way. Normal and neoplastic human breast tissues were investigated using OCE. Tissue sample was acquired from breast cancer patients under protocols approved by the institutional review boards of the University of Illinois at Urbana-Champaign and the Carle Foundation Hospital, Urbana, Illinois. The tumors were diagnosed as invasive ductal carcinomas via standard pathological evaluation techniques performed at Carle Foundation Hospital. The tissue samples were resected and placed in a buffered saline solution and stored in a cooler until imaging was performed 2 hours later. Both tumor tissue and normal adipose tissue were investigated using sinusoidal response OCE methods, and subsequently their Young's moduli were determined. Further more, tissue with both tumor and normal adipose was tested by sinusoidal response OCE method too, to show the Young's moduli distinguishing ability in this method.

3. RESULTS

Measured Young's moduli by three methods according to different silicone ingredients concentration ratios are shown in Table 1 and plotted in Figure 5. In this figure, we can see that as mass concentration ratio of specialty PDMS RTV-615A to pure PDMS fluid increases, the measured Young's moduli linearly increases as well, although the measured data from the three methods are not the same. Both step response and sinusoidal response OCE method data have linear calibration relationships in this range with indentation data, which is a standardized way of measuring Young's modulus of soft tissues, while the step response OCE method tends to increase more when the Young's modulus is high.

Table 1. Silicone phantom concentration ratios and measured Young's moduli by different methods

Phantom	1	2	3	4	5	6
Concentration Ratio	1:10:10	1:10:20	1:10:30	1:10:50	1:10:80	1:10:100
E_i(k Pa)	248.50	112.20	70.16	44.38	20.89	14.58
E_m(k Pa)	359.18	167.33	92.29	45.08	18.35	12.74
E_s(k Pa)	282.90	106.14	73.6	23.32	10.47	8.55

Concentration ratio of the phantom is the mass ratio of PDMS curing agent RTV-615B:specialty PDMS RTV-615A:pure PDMS fluid. E_i stands for Young's moduli measured by indentation method while E_m and E_s stand for Young's moduli measured by step response OCE and sinusoidal response OCE, respectively.

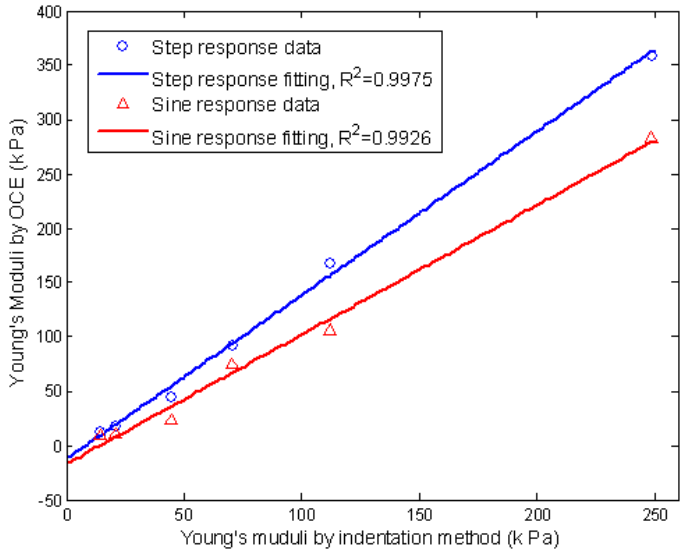

Figure 5. Measured Young's moduli results by three methods. Young's moduli measured by step response and sinusoidal response OCE methods are calibrated to standard indentation method.

Measured Young's moduli of breast adipose tissue and tumor tissue by sinusoidal response OCE method are shown in Table 2. Results from tissue with both tumor and normal adipose are measured. At different transverse positions of the tissue, the sinusoidal response OCE experiments were performed on the sample to test Young's moduli variation. Young's moduli were measured at 5 different transverse positions are shown in Table 2. From the results, we can see that tumor tissue has the Young's modulus about 25 times larger than the one of adipose tissue. When testing tissue with multiple types, we can tell a large variation of elastic moduli between tumor and adipose tissue, because tissues with different biomechanical properties have different responses to mechanical stimuli. However, due to simple mechanical model, these numbers are only relative values, which are not the real values of tissue's Young's moduli.

Table 2. Measured Young's moduli on tissues by OCE methods

Tissue/ Measurement Position	tumor	adipose	combination/ -1.5mm	combination/ -1.1mm	combination/ 0mm	combination/ 0.7mm	combination/ 1.2mm
E_s(k Pa)	10.68	0.42	4.14	2.69	4.59	12.92	14.15

OCE experiments investigated three types of tissue: tumor tissue only, adipose tissue only and the combination of tumor and adipose tissues. Measurement positions are indicating different transverse positions on the human breast tissue.

4. DISSCUSSION

An OCE system has been used for measuring Young's modulus of tissue phantoms and human breast tissues. Results have been correlated with biomechanical tissue models, and validated against a standard indentation method for determination of Young's modulus. With OCT technology, the novel OCE system has very high resolution in both axial and transverse directions and cross-correlation algorithm is no longer necessary.

From the results on silicone phantoms, we can see that measurements from three different methods (step response OCE, sinusoidal response OCE and indentation) are different, although they have linear relationships. Different strain rates in

these methods were believed to be the main reason for the measurement differences. It has been investigated that the elastic modulus of a biological sample was dependent on the strain rate of its deformation, because of the resistance originated from organic matrixes in the sample[14]. Thus, for our phantoms, the larger the strain rate is, the larger the Young's modulus will be measured. In our research, the strain rate for indentation method is 10 μm/s while strain rate for step response OCE is approximately 30 mm/s. The strain rates for sinusoidal response OCE are ranged approximately from 3 mm/s to 17 mm/s, depending on different samples. Basically, with strain rate much larger than the indentation method, the measured Young's moduli by OCE can be treated as "dynamic Young's moduli", which can be calibrated to standard "static Young's moduli" according to the linear relationship shown in Figure 5. In the range of 15 to 250 k Pa, we have the relationship of $E_m > E_s > E_i$.

Since OCT is a powerful high-speed *in vivo* imaging modality, our OCE system also has great potential to measure 3-D biomechanical properties of tissues and conduct *in vivo* studies. With these strong features and *in vivo* OCT imaging, our novel OCE technology can perform more accurately and with higher resolution in biomedical imaging field, such as breast tumor biopsy, intravascular imaging and atherosclerotic tissues imaging to help us understanding tissue biomechanical properties. Our OCE technology can be contributed to three dimensional dynamic engineered tissue imaging to detect the tissue reactions to different mechanical stimuli. This is significant for engineering new biological structures, biomaterials and biodevices.

5. Acknowledgement

We thank Drs. Dan Marks and Haohua Tu for their laboratory assistance with our optical systems. This work was supported in part by the National Science Foundation (BES 05-19920, S.A.B.), the National Institutes of Health (NIBIB, 1 R01 EB005221, and Roadmap Initiative, NIBIB, 1 R21 EB005321, S.A.B.), and Carle Foundation Hospital (S.A.B.). Additional information can be found at http://biophotonics.uiuc.edu.

6. Reference

[1] Fung Y.C., [Biomechanics: Mechanical Properties of Living Tissue], Springer-Verlag New York, Inc., 14-65 (1993).

[2] Ingber D.E., Dike L., Hansen L., Karp S., Liley H., Maniotis A., Mcnamee H., Mooney D., Plopper G., Sims J., et al., "Cellular tensegrity - exploring how mechanical changes in the cytoskeleton regulate cell-growth, migration, and tissue pattern during morphogenesis," Int. Rev. Cytol. 150:173-224 (1994).

[3] Shraiman B., "Mechanical feedback as a possible regulator of tissue growth," Proc Natl. Acad. Sci. USA 102:3318-3323 (2005).

[4] Dimitriadis E., Horkay F., Maresca J., Kachar B. and Chadwick R., "Determination of elastic moduli of thin layers of soft material using the atomic force microscope," Biophysical Journal 82:2798–2810 (2002).

[5] Devi C. U., Chandran R. S. B., Vasu R. M. and Sood A. K., "Measurement of visco-elastic properties of breast-tissue mimicking materials using diffusing wave spectroscopy," J. Biomed. Opt. 12(3):034035 (2007).

[6] Ophir J., Alam S. K., Garra B. S., Kallel F., Konofagou E. E., Krouskop T., Merritt C. R. B., Righetti R., Souchon R., Srinivasan S., et al., "Elastography: imaging the elastic properties of soft tissues with ultrasound," J. Med. Ultrasonics 29 (Winter):155-171 (2002).

[7] Wilson L. S.,Robinson D. E. and Dadd M. J., "Elastography - the movement begins," Phys. Med. Biol. 45:1409–1421 (2000).

[8] Schmitt J., "OCT elastography: imaging microscopic deformation and strain of tissue," Optics Express 3:199-211 (1998).

[9] Wang R. K., Kirkpatrick S. and Hinds M., "Phase-sensitive optical coherence elastography for mapping tissue microstrains in real time," Appl. Phys. Lett. 90:164105 (2007).

[10] van Soest G., Mastik F., de Jong N. and van der Steen A. F. W., "Robust intravascular optical coherence elastography by line correlations," Phys. Med. Biol. 52:2445-2458 (2007).

[11] Ko H., Tan W., Stack R. and Boppart S. A., "Optical coherence elastography of engineered and developing tissue," Tissue Engineering 12:63-73 (2006).

[12] Huber R., Adler D. C., and Fujimoto J. G., "Buffered Fourier domain mode locking: unidirectional swept laser sources for optical coherence tomography imaging at 370,000 lines/s," Opt. Lett. 31:2975-2977 (2006).

[13] Pogue B. W. and Patterson M. S., "Review of tissue simulating phantoms for optical spectroscopy, imaging and dosimetry," J. Biomed. Opt. 11(4):041102 (2006).
[14] Zhou J. and Hsiung L.L., "Biomolecular origin of the rate-dependent deformation of prismatic enamel," Appl. Phys. Lett. 89:051904 (2006).